Automated Vertical Design Optimization of a 1200V IGBT

A. Philippou, M. Bina, F.-J. Niedernostheide
Infineon Technologies AG
Am Campeon 1-12, D-85579 Neubiberg
Germany
Email: alexander.philippou@infineon.com

***Abstract*—Many important performance parameters in an IGBT power semiconductor are heavily affected by its field-stop profile, its device thickness and its collector-side p-doping concentration. To find the optimum combination of these design parameters is of high importance for an optimal IGBT design. The optimization criteria include low switching and on-state losses as well as limited maximum overshoot voltage and modest current and voltage rise and fall times. This work focusses on an automated global optimization scheme to solve this issue. The method and definition of a proper target function are briefly explained. Finally, design optimizations found under different constraints are discussed.**

I. Introduction

The desired switching profile of an IGBT is crucial for design optimization (e.g. [1], [2]). It has to be optimized for lowest switching losses, but at the same time exhibit only modest maximum overshoot voltage ($V_{\mathrm{ce,max}}$), combined with a low $\frac{dV}{dt}|_{10,90}$. For example a maximum $\frac{dV}{dt}|_{10,90}$ of $5\frac{kV}{\mu s}$ is required for drive applications. The term $\frac{dV}{dt}|_{10,90}$ denotes a voltage gradient calculated from points taken at 10% and 90% DC Link voltage V_{DC} on the rising edge. These requirements arise from electromagnetic compatibility (EMC) and interference (EMI) issues [3] as well as electric motor lifetime considerations [4]. While turn-off losses in general decrease with a reduced collector-side p-doping, $\frac{dV}{dt}|_{10,90}$ and the current gradient $\frac{dI}{dt}$ increase, as less carriers need to be extracted during turn-off. Consequently, the whole switching process is faster. The increased $\frac{dI}{dt}$ of this switching process results in a higher voltage overshoot $V_{\mathrm{ce,max}}$ induced by the stray inductance L_{s} of the system. A solution would be to increase the device thickness as this relaxes the requirement for $\frac{dV}{dt}|_{10,90}$, but increases switching losses again. Finally, the exact shape of the field-stop profile in combination with the base material doping has a huge impact on breakdown voltage, overshoot voltage, and switching losses simultaneously [5]. For example, increasing the doping concentration of a given field-stop profile might increase the reverse blocking voltage, which in turn could allow to reduce the device thickness. However, this in turn will result in an increased $V_{\mathrm{ce,max}}$. To automate this multidimensional design process, a global optimization approach via a modified simulated annealing scheme [6] is attractive.

II. Simulation Setup

For a standard turn-off event, a simple chopper circuit was selected, incorporating a stray inductance L_{s}. For each iteration in the annealing scheme, a complete turn-off simulation of the respective IGBT cell was performed utilizing the device simulator *Sentaurus Device*. In each isothermal simulation at 25 °C, the two-dimensional IGBT cell was switched off from $I_{\mathrm{nom}} = 140$ A, at a DC link voltage of $V_{DC} = 800$ V. The chopper circuit used in the simulations is illustrated in Fig. 1 together with a sketch of the IGBT cell.

TABLE I. Optimization Parameters

	σ_1	N_1	σ_2	x_2	N_2	d_p
Unit	μm	cm^{-3}	μm	μm	cm^{-3}	cm^{-2}
Min:	1.0	N_{min}	1.0	1.0	N_{min}	0.2×10^{13}
Max:	20.0	$60 \times N_{min}$	20.0	39.0	$30 \times N_{min}$	2.4×10^{13}

In order to optimize the design parameters of the IGBT for a low-power application and a high-power application, different stray inductance L_{s} have been used in the chopper circuit: 60 nH for the low-power application and 300 nH for the high-power application. The field-stop profile was parameterized via two Gaussian functions $G_1(\sigma_1, x_1 = 0, N_1)$ and $G_2(\sigma_2, x_2, N_2)$ where σ denotes the standard deviation, x the central position of the Gaussian function in μm from the backside, and N the peak concentration of the respective Gaussian function. The position of G_1 was fixed to the backside, as a final peak in front of the collector-side p-doped layer is necessary for a field-stop IGBT to prevent that the space-charge region expands into the p-doped layer during reverse blocking. Further optimization parameters include the collector-side p-doping dose d_{p}, as well as the device thickness x_{w} which was adjusted to fulfill the breakdown voltage requirements of a 1200V IGBT. The optimization parameters are shown in Tab. I.

TABLE II. Evaluation Parameters

	$\frac{dV}{dt}\|_{10,90}$	$V_{\mathrm{ce,max}}$	V_{r}	$V_{\mathrm{ce,sat}}$	E_{off}
Unit	$\frac{kV}{\mu s}$	V	V	V	mJ
Constraint	< 5.0	< 1150.0	< 20.0	1.4	10.0, 5.0

During each run the resulting switching profile was evaluated and several parameters were extracted. These evaluation parameters are shown in Tab. II. In order to assess the strength of ringing - i.e. the excitation of an oscillation in the V_{ce}-transient that is induced by a large current-decrease rate in the resonant circuit formed by the stray inductance and the device capacitance - we used the quantity V_{r}. It is defined as the amplitude of the first half cycle of the excited V_{ce} oscillation

978-1-4673-7860-4/15/$31.00 ©2015 IEEE

appearing after the voltage overshoot (cf. Fig. 2). The target values of the turn-off losses E_{off} were set to relatively low values, namely 5.0 mJ and 10.0 mJ for the low-power and the high-power case, respectively. All other bounds remained the same for both optimizations.

The evaluation parameters entered into a target function f based on a sum over relative errors

$$f = \sum_i \gamma_i \left(\frac{x_i - x^t{}_i}{x^t{}_i} \right)^2 + P(x_i, x^c{}_i) \tag{1}$$

where x_i denotes the i-th evaluation parameter, $x^t{}_i$ its target value, and γ_i an additional weighting factor for each parameter. Here $P(x_i, x^c{}_i)$ defines a penalty function

$$P(x_i, x^c{}_i) = \kappa_i \left| \text{erfc} \left(\left| \frac{x_i}{x^c{}_i} \right| \right) \right| \tag{2}$$

where $x^c{}_i(x^t{}_i)$ is the corresponding violated bound of the i-th parameter, κ_i its corresponding penalty weight, and erfc is the complimentary error function. After the target function was computed, a new parameter set was chosen according to the simulated annealing scheme and the annealing temperature was lowered by a cooldown factor $\alpha \in (0, 1)$, usually close to 1. The simulated annealing scheme for a single iteration j at a given value of the target function $f_j(\vec{x}_j)$ for a parameter set $\vec{x}_j$ and annealing temperature T_j can therefore be summarized as:

- Randomly determine new trial parameter set $\vec{x}_{tr}$.
- Compute trial value $f_{tr}(\vec{x}_{tr})$.
- If $f_{tr} \leq f_j$:
  - $\vec{x}_j \leftarrow \vec{x}_{tr}$
  - $T_j \leftarrow \alpha\ T_j$
- Else: Draw uniform random number $r \in [0, 1]$.
  - If $r < e^{-(f_{tr} - f_j)/T_j}$: $\vec{x}_j \leftarrow \vec{x}_{tr}$, $T_j \leftarrow \alpha\ T_j$
  - Else: $T_j \leftarrow \alpha\ T_j$ (reject trial parameters)
- $j \leftarrow j + 1$

A flow of the whole optimization procedure is displayed in Fig. 3. Optimization runs with 250 iterations each have been performed. The computational speed of the optimization strongly depends on the capability of the device simulator to solve the turn-off transient of the IGBT quickly. In our case a single optimization iteration took around 10 minutes.

III. High-Power IGBT Variant

The resulting decrease of the target function for the high-power case is shown in Fig. 4 and plotted together with the applied simulated annealing temperature. An almost global minima was already found after 50 iterations, but due to the still high simulated annealing temperature further configurations were evaluated. At the end, the solution fluctuated around the previously found configuration, thus reaching the global minima in iteration 246. The run continued until iteration 250. At the end, the global minima from iteration 246 was written out. For selected iterations of this optimization run, transient switching profiles were extracted (Fig. 5). While the profiles at iteration 21 and iteration 109 exhibited a fast switching with

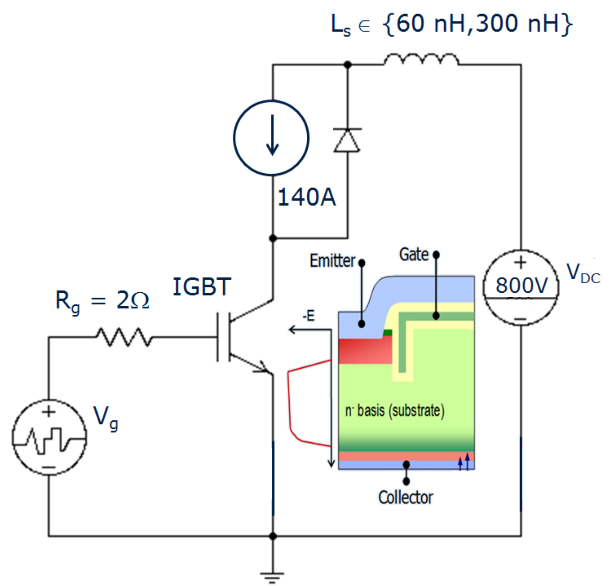

Fig. 1. Chopper circuit together with a schematic of the IGBT cell used for turn-off simulations during each optimization iteration.

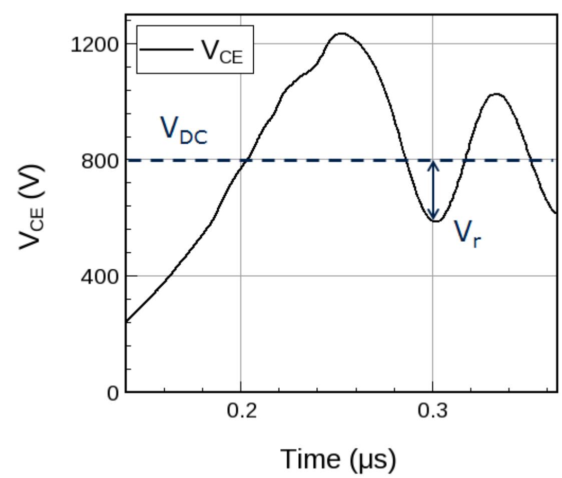

Fig. 2. Turn-off example showing the definition of V_r for a high stray inductance.

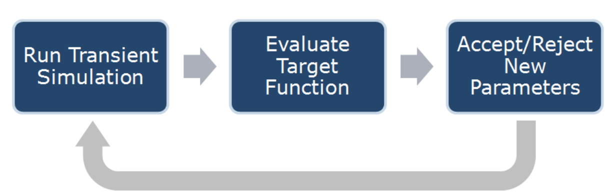

Fig. 3. A schematic of the processes of an optimization run.

lower turn-off losses, they violated several constraints, such as the $V_{\mathrm{ce,max}}$ limit.

A more detailed analysis of the contribution of each term to the target functions at the three selected iterations is presented

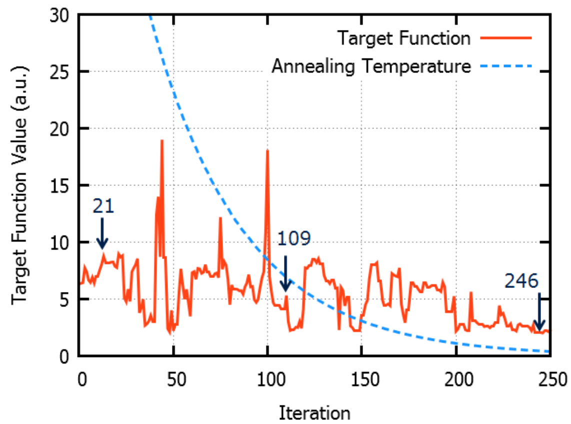

Fig. 4. An optimization run with the simulated annealing scheme. At the points marked by an arrow switching curves were extracted.

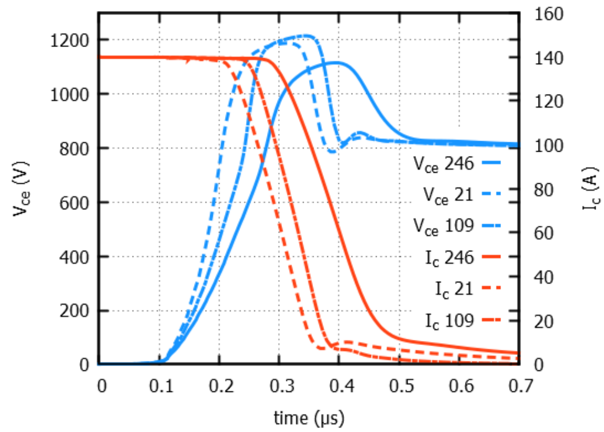

Fig. 5. Switching transients of IGBTs with interim field-stop profiles after iterations marked in Fig. 4.

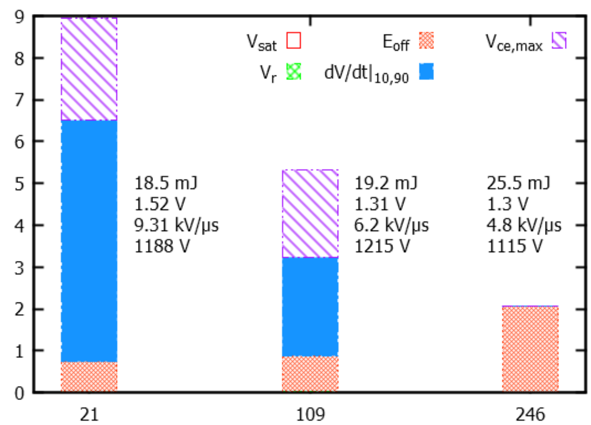

Fig. 6. Contribution of each term to the target function f after the iterations marked in Fig. 4. Also shown are the values of $V_{\mathrm{ce,sat}}$, E_{off}, $\frac{dV}{dt}|_{10,90}$, and $V_{\mathrm{ce,max}}$ respectively at each position.

in Fig. 6. The profile at iteration 21 violated especially the $\frac{dV}{dt}|_{10,90}$ and $V_{\mathrm{ce,max}}$ constraint, resulting in large penalties. As the optimization continued, these penalties could be reduced, while keeping an almost constant E_{off} with a reduction of $V_{\mathrm{ce,sat}}$ from $1.5V$ to $1.3V$ (iteration 109). However, only for the final profile, the $\frac{dV}{dt}|_{10,90}$ and $V_{ce,max}$ constraints could be met, in this case at the cost of an increased E_{off}. The final switching curve is shown in more detail in Fig. 7. The $\frac{dV}{dt}|_{10,90}$ value was below $5\frac{kV}{\mu s}$, but for example the $\frac{dV}{dt}|_{\max}$ value, defined as the maximum occuring $\frac{dV}{dt}$, is higher. If it is necessary to reduce this value, it must be included into the target function. This also demonstrates a crucial aspect of the whole optimization scheme: A careful definition of the contribution of each term of the target function and the penalty function is very important, because they define the final device performance.

IV. Low-Power IGBT Variant

For the low-power case, a different optimium was found. While a similar decrease of the target function throughout the optimization as in the high-power case could be observed, the resulting device parameters after 250 iterations were substantially different from those obtained in the high-power case. As L_{s} for the low-power IGBT variant was considerably lower than in the high-power case, penalties in $V_{ce,max}$ where less pronounced, allowing the optimization algorithm to decrease the device thickness and allow for a faster switching. The resulting optimized field-stop profile is shown in Fig. 8 together with that of the optimized high-power IGBT variant. While the high-power field stop reaches deeper into the device to allow for a slower build up of the electric field during turn-off, the low-power field stop is much more confined to the backside and more strongly doped to stop the field more aggressively and prevent a punch through as a result of the reduced device thickness. The final transient switching curves for the low-power IGBT variant are shown in Fig. 9 together with its extracted evaluation parameters which entered the target function.

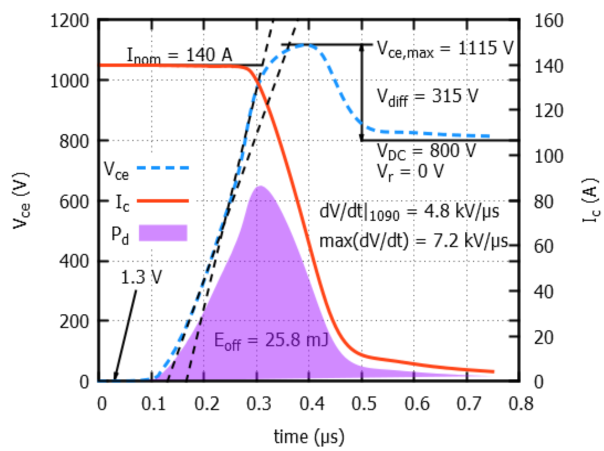

Fig. 7. Turn-off transients of the optimized device for the high-power IGBT variant ($L_{\mathrm{s}} = 300$ nH); the dyed area marks the power dissipation P_{d}.

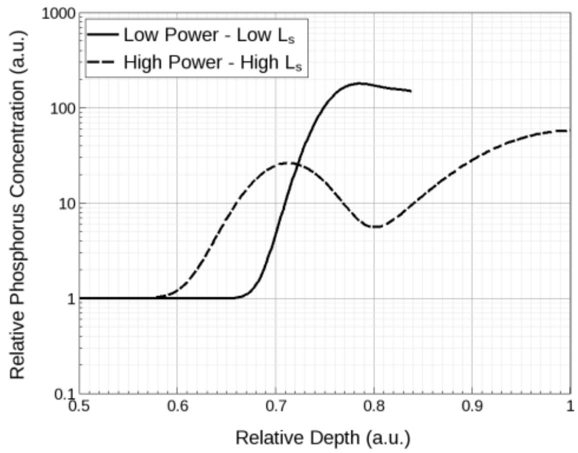

Fig. 8. Resulting field-stop profiles of the low-power and the high-power IGBT variant obtained for the two different stray inductance after optimization.

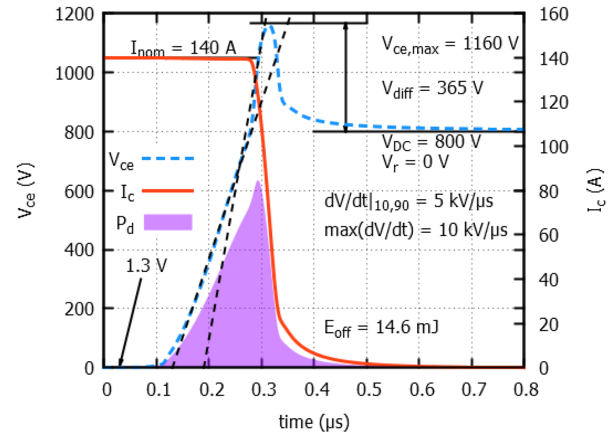

Fig. 9. Turn-off switching characteristic of low-power IGBT variant (L_s = 60 nH); the dyed area marks the power dissipation P_d.

V. Conclusion

An automated scheme based on a simulated annealing algorithm was developed and applied to optimize the vertical design of a 1200V IGBT with respect to numerous constraints. Specific design solutions for high-power and low-power applications were derived. The optimization is based on the assessment of the IGBTs turn-off characteristics. The computational speed for a single transient switching calculation based on two-dimensional device simulation is crucial for the practicability of the presented method. The optimization algorithm can easily be extended to include also the assessment of the turn-on behavior or other criteria, for example the switching behavior at different DC link voltages or currents. The definition of the target function to be minimized during the optimization process is of great importance, as the contributions and the penalties associated with each term of the target function determine the final design performance.

References

[1] T. Laska, M. Munzer, F. Pfirsch, C. Schaeffer, T. Schmidt, *The Field Stop IGBT (FS IGBT). A new power device concept with a great improvement potential*, Proc. ISPSD '00, pp. 355-358, 2000.

[2] A. P.-S. Hsieh, G. Camuso, F. Udrea, Yi Tang, Chiu Ng, N. Ranjan, A. Charles, *Field-stop layer optimization for 1200V FS IGBT operating at 200 C*, Proc. ISPSD '14, pp. 115-118, 2014.

[3] Q. Lid, W. Shen, F. Wang, D. Boroyevich, V. Stefanovic, M. Arpilliere, *Experimental Evaluation of IGBTs for Characterizing and Modeling Conducted EMI Emission in PWM Inverters*, Power Electronics Specialists Conference, vol. 4., pp. 1951-1956, 2003.

[4] J. M. Erdman, R. J. Kerkman, D. W. Schlegel, and G. L. Skibinski, *Effect of PWM inverters on ac motor bearing currents and shaft voltages*, IEEE Trans. Ind. Appl., vol. 32, pp. 250259, 1996.

[5] H. G. Eckel, K. Fleisch, *Turn-off behaviour of high voltage NPT- and FS-IGBT*, 13th EPE-PEMC, pp. 48-53, 2008.

[6] P. J. M. van Laarhoven, E. H. L. Aarts, *Simulated Annealing: Theory and Applications*, Kluwer Academic Publishers, 1987.